February 1, 2008

CP violation in top quark production at the LHC and Two-Higgs-Doublet Models

Wafaa Khater and Per Osland

Department of Physics, University of Bergen, Allegt. 55, N-5007 Bergen, Norway

Abstract

We discuss CP violation in top-antitop production at the LHC, induced by gluon fusion and final-state Higgs exchange. Results by Bernreuther and Brandenburg are confirmed and further reduced. The lepton energy asymmetry is studied in detail in explicit Two-Higgs-Doublet Models with near-maximal mixing in the neutral Higgs sector. Unless there is *only one light Higgs particle*, and unless (in "Model II") $\tan\beta \lesssim 1$, the CP-violating effects are very small, possibly too small to be seen at the LHC.

1 Introduction

One of the most promising ways in which one can search for new physics at the LHC, is in CP violation in connection with $t\bar{t}$ production. It is generally believed that the top quark, since it is very heavy, might be more susceptible to new physics [1, 2]. In the particular case of Higgs-mediated interactions, this is naturally the case, since the Higgs coupling to the top quark is proportional to its mass. This process

$$pp \to t\bar{t} + X \tag{1.1}$$

has been explored in considerable detail by Bernreuther and Brandenburg [3, 4] who identified the different kinematical structures appearing in the CP-violating part of the interaction, and evaluated them in a generic Two-Higgs-Doublet Model [5].

Here, we review (and confirm) these calculations, and apply the results to a particular version of the Two-Higgs-Doublet Model, in which the CP violation is minimal in structure [6]. This allows us to relate and constrain the couplings and masses of the model. Such relations among parameters are crucial in order to estimate the magnitude of possible signals.

If the Higgs states are not eigenstates under parity, then their couplings to the fermions will violate CP. In particular, if the $Ht\bar{t}$ coupling (for a given Higgs particle) is of the generic form

$$Ht\bar{t}: \qquad [a + i\gamma_5\tilde{a}], \tag{1.2}$$

then the CP-violating part of the cross section for the process (1.1), which depends on the t and $\bar{t}$ spins, will be proportional to the dimensionless model-dependent quantity

$$\gamma_{CP} = -a\tilde{a} \tag{1.3}$$

where a, $\tilde{a}$ are the reduced scalar and pseudoscalar Yukawa couplings, respectively.

Here, we restrict ourselves to the subprocess $gg \to t\bar{t}$ since it is the leading $t\bar{t}$ production mechanism at the CERN LHC. The $q\bar{q}$ initial states, which are important at the Tevatron [3], contribute at the LHC less than 10% to the total cross section [7] and give only a numerically negligible contamination of the CP-violating signal [1, 3].

The MSSM provides an alternative, very interesting framework for CP violation via the Higgs sector [8]. Additional effects in the MSSM include CP-violating gluino exchange [9, 10] as well as those due to phases in the bilinear and trilinear couplings, given by the so-called μ and A_t parameters. For an application to the process (1.1), see [10]. We here restrict ourselves to the 2HDM, this is already a rich framework.

The paper is organized as follows. After a review of notation and relevant formulas in sect. 2, we give model-independent results in sect. 3, focusing on basic observables discussed in [3]. In sect. 4, we review the physical content of the 2HDM, and in sect. 5, we study the magnitude of the CP violation for two distinct neutral Higgs mass spectra: two light

and one heavy *vs.* one light and two heavy. Sect. 6 is devoted to concluding remarks, and an appendix summarizes the basic one-loop results for the CP-violating amplitudes.

2 Preliminaries

A schematic representation of a generic one-loop diagram of the process $gg \to t\bar{t}$ is given in fig. 1.[1]

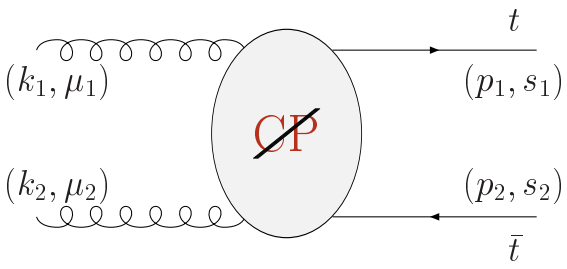

Figure 1: Kinematics of the underlying $g(k_1) + g(k_2) \to t(p_1) + \bar{t}(p_2)$ reaction.

2.1 Notation

The momentum and the spin four-vectors of the top (and antitop) quark are denoted by p_1 and s_1 (and p_2 and s_2), respectively, with m_t the mass, whereas the momenta and the Lorentz indices of the initial gluons are represented by k_i and μ_i $(i = 1, 2)$. We introduce the linearly-independent set of momenta (P_g, Q, P_t):

$$Q = k_1 + k_2 = p_1 + p_2, \qquad P_g = k_1 - k_2, \qquad P_t = p_1 - p_2, \tag{2.1}$$

with $Q \cdot P_t = Q \cdot P_g = 0$. The non-vanishing scalar products involving the momenta (P_g, Q, P_t) are given by $Q^2 = -P_g^2 = \hat{s}$, $P_t^2 = -\beta^2 \hat{s}$ and $(P_g \cdot P_t) = -\beta z \hat{s}$ where $\hat{s}$ is the gluon–gluon center of mass energy squared, $\beta = \sqrt{1 - 4m_t^2/\hat{s}}$ is the top quark velocity and $z = \cos\theta = (\hat{\mathbf{P}}_g \cdot \hat{\mathbf{P}}_t)$, with θ the scattering angle in the gluon–gluon center of mass frame. Working with the linearly-independent set of momenta (P_g, Q, P_t) simplifies the kinematics, the four-point first- and second-rank tensor loop integrals in particular.

[1] To produce the figures, the AXODRAW package [11] was used.

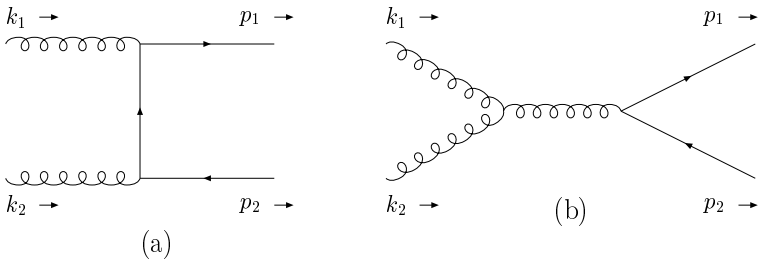

Figure 2: Lowest-order QCD Feynman diagrams of the underlying $gg \to t\bar{t}$ reaction, the crossed diagram of (a) is not shown.

Denoting by $\mathcal{M}_0$ the QCD amplitude corresponding to the diagrams of fig. 2, and by $\mathcal{M}_1$ the one corresponding to the one-loop Higgs-exchange diagrams of fig. 3, we obtain the cross section

$$\sigma \propto |\mathcal{M}_0 + \mathcal{M}_1|^2. \tag{2.2}$$

Spin-dependent CP-violating parts arise from terms linear in γ_{CP}, (1.3). Those originate from interference between $\mathcal{M}_0$ and $\mathcal{M}_1$, and from $|\mathcal{M}_1|^2$.[2] We write

$$\sigma = \sigma_{\rm even} + \sigma_{CP}, \tag{2.3}$$

where the non-interesting CP-even part of the cross section $\sigma_{\rm even}$ results from $|\mathcal{M}_0|^2$ and from the terms in $|\mathcal{M}_1|^2$ that are independent of γ_{CP} or *even* in this quantity. The CP-violating part of the cross section can be written in the most general Lorentz-invariant form as

$$\begin{aligned}\sigma_{CP} \propto\ & \Phi_1[P_g \cdot s_1 - (1 \leftrightarrow 2)] + \Phi_2[P_t \cdot s_1 - (1 \leftrightarrow 2)] + \Phi_3[R \cdot s_1 - (1 \leftrightarrow 2)] \\ & + \Psi_1[(R \cdot s_1)(P_g \cdot s_2) - (1 \leftrightarrow 2)] + \Psi_2[(R \cdot s_1)(P_t \cdot s_2) - (1 \leftrightarrow 2)] \\ & + \Psi_3[(P_g \cdot s_1)(P_t \cdot s_2) - (1 \leftrightarrow 2)],\end{aligned} \tag{2.4}$$

with the auxiliary pseudovector

$$R_\sigma = \epsilon_{\mu\nu\rho\sigma} P_g^\mu Q^\nu P_t^\rho. \tag{2.5}$$

[2]When calculating linear terms in γ_{CP} in $|\mathcal{M}_1|^2$, we only considered the contribution from diagram h in fig. 3, which is important for m_H above the $t\bar{t}$ threshold [4].

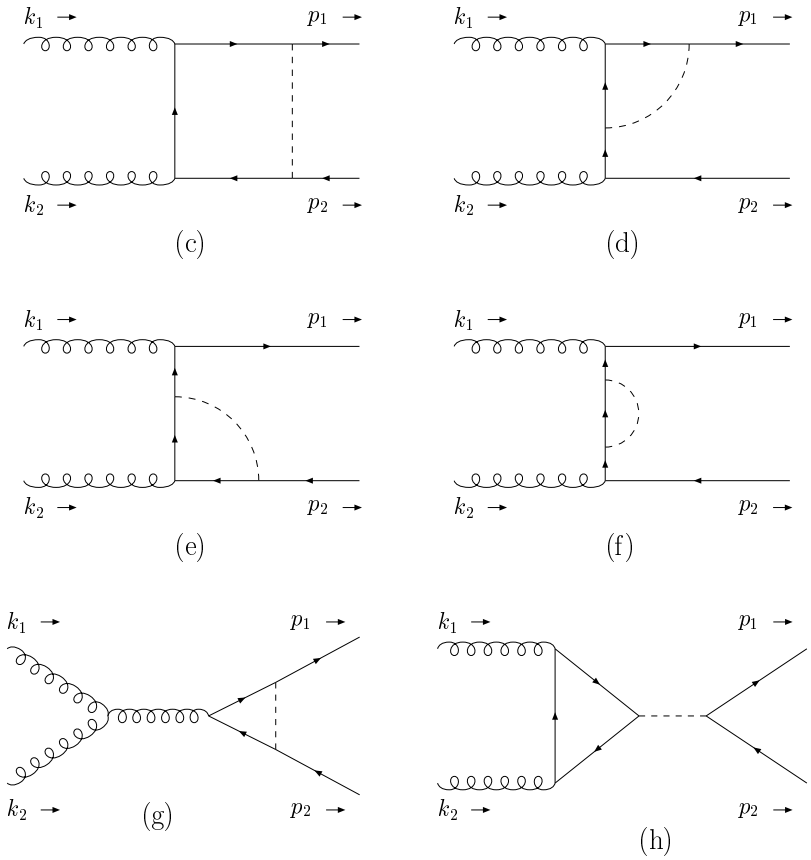

Figure 3: Feynman diagrams of the underlying $gg \to t\bar{t}$ reaction with neutral non-Standard-Model Higgs exchanges (dashed). The crossed diagrams are not shown (diagram (g) has no crossed partner).

The coefficients $\Phi_1, \ldots \Phi_3$ and $\Psi_1, \ldots \Psi_3$, the structure of which are determined by the actual Higgs exchange diagrams (for details, see [3, 17]), depend on $\hat{s}$, z and the masses of the Higgs boson and the top quark, m_H and m_t.

2.2 The Bernreuther–Brandenburg decomposition

Bernreuther and Brandenburg describe the CP violation in the process of fig. 1 in terms of the $t\bar{t}$ production density matrix, eq. (2.8) in [3] as:

$$\mathcal{R}_{CP} = (b_{g1}^{CP}\hat{k}_i + b_{g2}^{CP}\hat{p}_i + b_{g3}^{CP}\hat{n}_i)(\sigma^i \otimes \mathbf{1} - \mathbf{1} \otimes \sigma^i) + \epsilon_{ijk}(c_{g1}\hat{k}_i + c_{g2}\hat{p}_i + c_{g3}\hat{n}_i)\sigma^j \otimes \sigma^k, \quad (2.6)$$

where (in our notation) $\hat{\mathbf{k}} = \hat{\mathbf{P}}_g$, $\hat{\mathbf{p}} = \hat{\mathbf{P}}_t$ and $\hat{\mathbf{n}}$ is the unit vector in the direction of $\mathbf{n} = \mathbf{P}_g \times \mathbf{P}_t$ defined in the gluon–gluon center of mass frame.[3] The σ^i are Pauli matrices with $\mathbf{s_1} = \frac{1}{2}\boldsymbol{\sigma} \otimes \mathbf{1}$ ($\mathbf{s_2} = \frac{1}{2}\mathbf{1} \otimes \boldsymbol{\sigma}$) the spin operator of the top (anti-top) defined in the top (anti-top) rest frame.

The relation of this expansion to our eq. (2.4) is given by:

$$\begin{aligned}
b_{g1}^{CP} &= -\sqrt{\hat{s}}\,\Phi_1, \\
b_{g2}^{CP} &= -\sqrt{\hat{s}}\left(\frac{\sqrt{\hat{s}}}{2m_t} - 1\right) z\,\Phi_1 - \frac{\hat{s}}{2m_t}\,\beta\,\Phi_2, \\
b_{g3}^{CP} &= \hat{s}\sqrt{\hat{s}}\,\beta\sqrt{1-z^2}\,\Phi_3, \\
c_{g1} &= \frac{\hat{s}^2\sqrt{\hat{s}}\,\beta}{2m_t}[z\Psi_1 + \beta\,\Psi_2], \\
c_{g2} &= -\frac{\hat{s}^2\sqrt{\hat{s}}\,\beta z}{2m_t}[z\Psi_1 + \beta\,\Psi_2] - \hat{s}^2\beta(1-z^2)\Psi_1, \\
c_{g3} &= \frac{\hat{s}\sqrt{\hat{s}}}{2m_t}\beta\sqrt{1-z^2}\,\Psi_3.
\end{aligned} \tag{2.7}$$

The symmetry properties of these functions are given in [3].

We confirm the results for these functions (2.7) given in the appendix of ref. [3], up to some misprints mentioned in [4]. Also, we have further reduced the results of the box diagram to the basic four-point function together with three- and two-point functions. This yields a more unique representation, and is also convenient for the use of standard loop function libraries, like the "LoopTools" package [13, 14]. Our results are collected in Appendix A.

3 Model-independent results

Before invoking concrete models, we shall first update and review some CP-violating quantities discussed in [3], both at the parton level and at the hadronic level.

[3]For the momenta of the partons involved, we use the notation $g(k_1) + g(k_2) \to t(p_1) + \bar{t}(p_2)$, while in [3] the notation $g(p_1) + g(p_2) \to t(k_1) + \bar{t}(k_2)$ was used.

3.1 CP violation at the parton level

We first consider the non-vanishing[4] parton-level CP-odd quantities [3]:

$$\langle \hat{\mathbf{p}} \cdot (\boldsymbol{s}_1 - \boldsymbol{s}_2) \rangle_g = \frac{4 \int_{-1}^{1} dz (z b_{g1}^{CP} + b_{g2}^{CP})}{4 \int_{-1}^{1} dz\, A^g}, \tag{3.1}$$

$$\langle \hat{\mathbf{p}} \cdot (\boldsymbol{s}_1 \times \boldsymbol{s}_2) \rangle_g = \frac{2 \int_{-1}^{1} dz (z c_{g1}^{CP} + c_{g2}^{CP})}{4 \int_{-1}^{1} dz\, A^g}, \tag{3.2}$$

where A^g is the spin-independent part of the CP-even part of the production density matrix given analytically in [3]. We note that these two spin–spin correlations are given by absorptive and dispersive parts of the amplitudes (see Appendix A). Plots of these expectation values *vs.* the center of mass energy $\sqrt{\hat{s}}$ are shown in fig. 4.

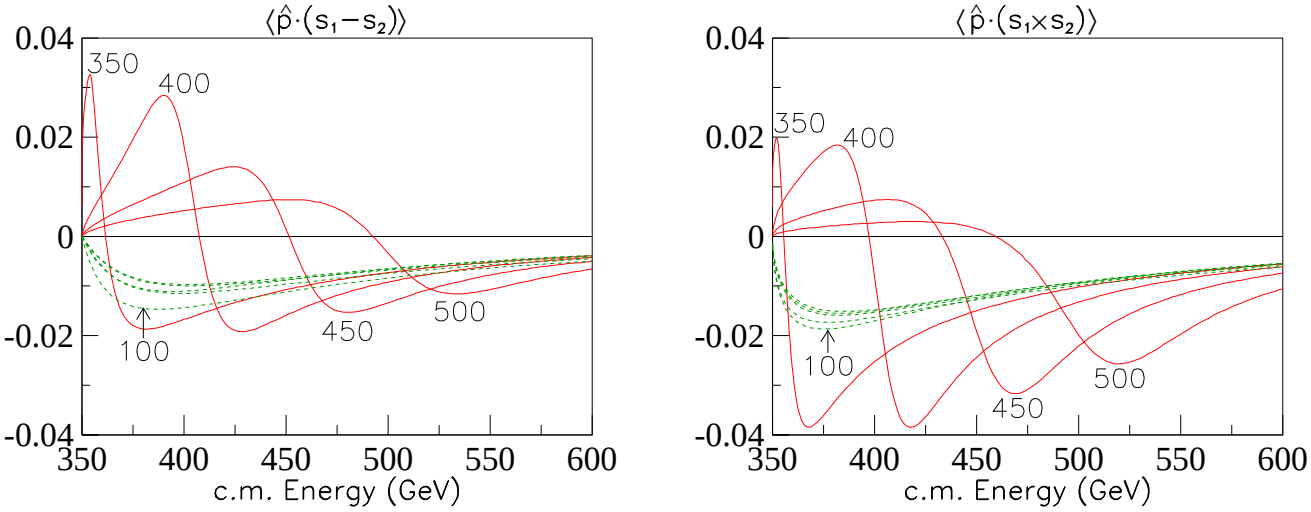

Figure 4: Parton-level spin-spin correlations (3.1) and (3.2) in $gg \to t\bar{t}$ *vs.* $\sqrt{\hat{s}}$, for $\gamma_{CP} = 1$ and different Higgs masses. Dashed: $m_H = 100, 150, \ldots, 300$ GeV; solid: $350, \ldots, 500$ GeV.

We confirm the results of [3] for (3.1) (fig. 4, left panel), but differ from their results for (3.2) (fig. 4, right panel), since there were sign misprints in the structure functions $c_{g_1}^{(f)}$ and $c_{g_2}^{(f)}$ and a wrong factor of 8π in the Higgs width Γ_Z used in [3] and corrected in [4]. In our numerical work, we used the "LoopTools" package [13, 14].

[4]The corresponding quantities involving the gluon or beam direction, vanish due to the symmetry properties under z.

As stressed in [4], for Higgs masses above the $t\bar{t}$ threshold, the quantity (3.1) (and to a lesser extent (3.2)) has a characteristic "resonance–interference" shape, with peaks in the region $\sqrt{\hat{s}} \sim m_H$. As one goes from $\sqrt{\hat{s}} \lesssim m_H$ to $\sqrt{\hat{s}} \gtrsim m_H$ the expectation values (3.1) and (3.2) change sign. Thus, there are cancellations which tend to reduce the CP-violating effects, when folded with the gluon distribution functions, i.e., when integrated over the $t\bar{t}$ invariant mass, $M_{t\bar{t}} = \sqrt{\hat{s}}$.

3.2 Observables in $pp \to t\bar{t}X \to l^+l^-X$

We consider events where the t and/or the $\bar{t}$ quarks decay semileptonically:

$$t \to l^+ \nu_l b, \quad \bar{t} \to l^- \bar{\nu}_l \bar{b}, \tag{3.3}$$

and denote the lepton laboratory-frame momenta and energies by $\mathbf{l}^\pm$ and $E_\pm$. Following ref. [3], we neglect any CP violation in the top decay. This effect has been found to be small [15, 16].

For reference, we shall consider the observables [3]

$$A_1 = E_+ - E_-, \tag{3.4}$$

$$A_2 = \mathbf{p}_{\bar{t}} \cdot \mathbf{l}^+ - \mathbf{p}_t \cdot \mathbf{l}^-, \tag{3.5}$$

where $\mathbf{p}_t$ ($\mathbf{p}_{\bar{t}}$) is the top (anti-top) three-momentum in the laboratory frame. The lepton energy asymmetry, A_1, requires events where *both* the top and the anti-top decay semileptonically. The observable A_2 requires the top or antitop to decay hadronically, while the other decays semileptonically. From the two-sample scenario discussed in [4] with sample $\mathcal{A}$ consisting of events where the t decays semileptonically and the $\bar{t}$ decays hadronically and sample $\bar{\mathcal{A}}$ where the t decays hadronically and the $\bar{t}$ decays semileptonically, one defines the expectation value of the asymmetry A_2 as

$$\langle A_2 \rangle = \langle \mathbf{p}_{\bar{t}} \cdot \mathbf{l}^+ \rangle_{\mathcal{A}} - \langle \mathbf{p}_t \cdot \mathbf{l}^- \rangle_{\bar{\mathcal{A}}}. \tag{3.6}$$

In fig. 5 we show the expectation value $\langle A_1 \rangle$, together with the ratio[5]

$$\frac{S}{N} = \frac{\langle A_1 \rangle}{\sqrt{\langle A_1^2 \rangle - \langle A_1 \rangle^2}} \tag{3.7}$$

[5]We shall loosely refer to this as "signal-to-noise ratio" [3].

both as functions of the Higgs mass, and for $\gamma_{CP} = 1$. The right panel here corresponds to fig. 7 of ref. [3], but for $m_t = 175$ GeV.[6] Here, and throughout this paper, we have used the CTEQ6 parton distribution functions [12]. The fact that $S/N = \mathcal{O}(10^{-3})$ means that of the order of a million $t\bar{t}$ events are required (in the dilepton channel). Also, it means that the relative lepton energy must be known at (or better than) the per mille level.

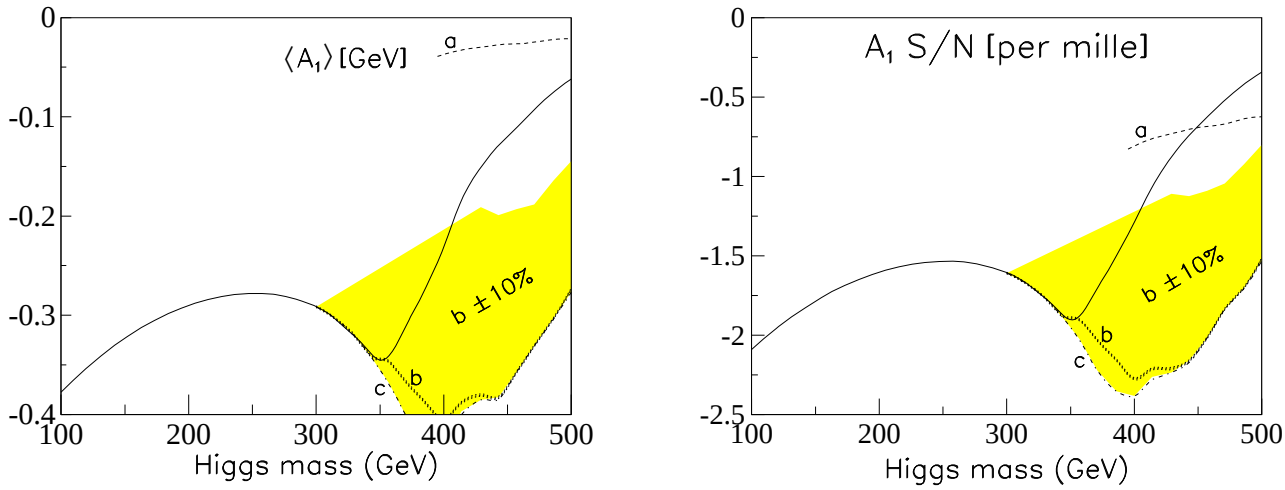

Figure 5: *Left panel:* Lepton energy correlations $\langle A_1 \rangle$ in $pp \to t\bar{t}X$ *vs.* Higgs mass for $\gamma_{CP} = 1$. Dashed curves labeled "a", "b" and "c" refer to modified observables of eq. (3.8). Grey (yellow) band: $\langle A_1^{(b)} \rangle$, with 10% uncertainty in $M_{t\bar{t}}$. *Right panel:* Corresponding signal-to-noise ratio.

Next, we turn to the observable A_2. We reproduce the analytical result of [3], their eq. (4.5), but our numerical result, shown in fig. 6, has the opposite sign, and the signal-to-noise ratio is in magnitude smaller than theirs by a factor of $\mathcal{O}(1/10)$ [17]. Thus, the observable A_2 may be rather hard to access at the LHC.

The reason for the small signal-to-noise ratio for A_2 (as compared to A_1) appears to be a combination of two effects. The main effect is due to the Lorentz transformations. Since it is bilinear in momenta, factors like $B_2 = 1/(1-\beta_{gg}^2)$ and $B_2' = \beta_{gg}^2/(1-\beta_{gg}^2)$ are involved, *vs.* $B_1 = 1/\sqrt{1-\beta_{gg}^2}$ for A_1, with β_{gg} the gluon–gluon c.m. velocity w.r.t. the laboratory frame. The "signal-to-noise" ratios for these quantities ("quasi-observables")

[6] We reproduce their results for the same choice of m_t and the same Higgs widths. Also, we note that a factor of β is missing in eq. (4.4) of [3].

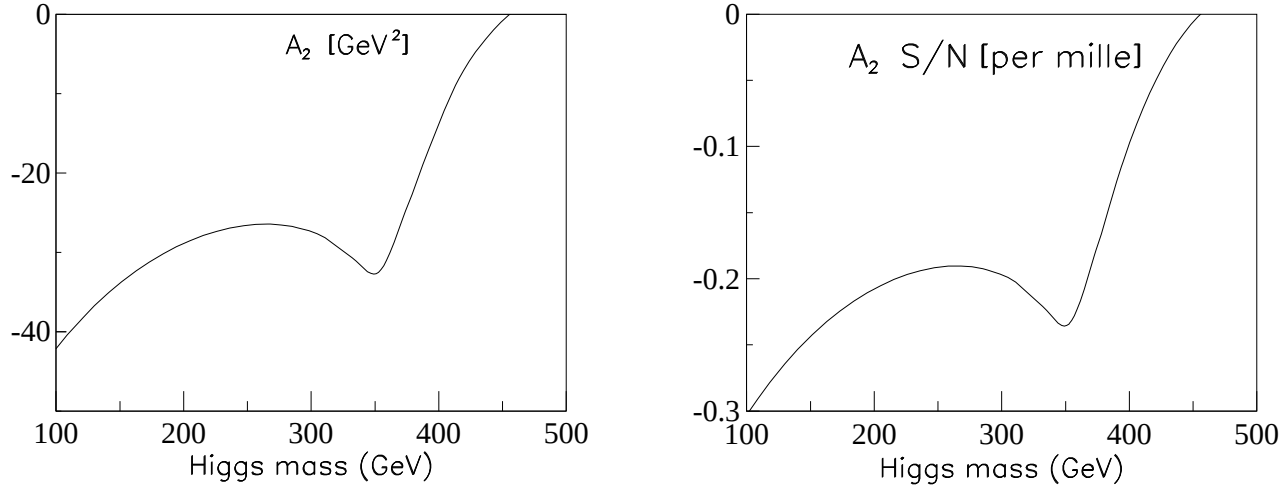

Figure 6: *Left panel:* Momentum–momentum correlations $\langle A_2 \rangle$ (see eq. (3.5)) in $pp \to t\bar{t}X$ *vs.* Higgs mass for $\gamma_{CP} = 1$. *Right panel:* Corresponding signal-to-noise ratio.

B_2 and B_2' are reduced with respect to that of B_1 by a factor of 3–4. This is due to the importance of events where the $t\bar{t}$ invariant mass is close to threshold, and the relatively light $t\bar{t}$ system has a high velocity in the laboratory system. Furthermore, in A_2, higher powers of cosines of angles are involved, and we note that, for example, $\langle \cos^2 \theta \rangle = 1/3$, whereas $\langle \cos^4 \theta \rangle = 1/5$. Together, these two effects give a reduction by $\mathcal{O}(1/10)$.

For values of the Higgs mass above the $t\bar{t}$ threshold, there is a fall-off in the absolute value of S/N. This is in part due to cancellation between the positive and negative parts in $\langle \hat{\mathbf{p}} \cdot (\mathbf{s}_1 - \mathbf{s}_2) \rangle$, as shown in fig. 4. One possible way to enhance the signal, would be to consider bins in $M_{t\bar{t}}$, centered around the resonant contribution of the (lightest) Higgs particle [4]. It would be worthwhile to perform a detailed simulation study of the gains of such binning in $M_{t\bar{t}}$. The value of this technique would depend critically on the mass resolution that can be achieved by a given detector.

We have investigated various other ways to reduce this loss of sensitivity, by studying instead of A_1, the modified observables (still for events with two leptons):

$$A_1^{(a)} = \frac{M_{t\bar{t}} - M_H}{M_{t\bar{t}} + M_H} A_1, \tag{3.8}$$

$$A_1^{(b)} = \mathrm{sign}(M_{t\bar{t}} - M_H)\, A_1, \tag{3.9}$$

$$A_1^{(c)} = -|A_1|. \tag{3.10}$$

The expectation values and signal-to-noise ratios for these observables are also shown in fig. 5, labeled "a", "b" and "c". For $A_1^{(b)}$, and for high Higgs masses, a significant improvement is obtained. However, the modified observables $A_1^{(a)}$ and $A_1^{(b)}$ require precise knowledge of the $t\bar{t}$ invariant mass, as well as of the Higgs mass. Of these, presumably the $t\bar{t}$ invariant mass will be the most difficult one to determine. We show in fig. 5 the ranges in $\langle A_1^{(b)} \rangle$ and signal-to-noise ratio that result from errors of 10% in this invariant mass.

If only the magnitude of A_1 is required, then it can be determined with better sensitivity from $A_1^{(c)} = -|A_1|$, which in fig. 5 coincides with the lower boundary of the shaded region and hence gives the largest signal enhancement.

4 The Two-Higgs-Doublet Model

In the previous discussion, the amount of CP violation was given by the Yukawa couplings a, $\tilde{a}$ (in particular, via the product, $\gamma_{CP} = -a\tilde{a}$) and the Higgs mass. In an explicit model, the situation is more complex, since there are several Higgs bosons, whose masses and couplings will be inter-related by the specific model. As an example of such a more complex situation, we shall in this and the next section study a specific Two-Higgs-Doublet Model where the CP violation is *minimal* in structure.

4.1 Parametrization

The Two-Higgs-Doublet Model we want to consider, is the one discussed in [6], where the potential is given by

$$\begin{aligned} V &= \frac{\lambda_1}{2}(\phi_1^\dagger\phi_1)^2 + \frac{\lambda_2}{2}(\phi_2^\dagger\phi_2)^2 + \lambda_3(\phi_1^\dagger\phi_1)(\phi_2^\dagger\phi_2) + \lambda_4(\phi_1^\dagger\phi_2)(\phi_2^\dagger\phi_1) \\ &\quad + \frac{1}{2}\left[\lambda_5(\phi_1^\dagger\phi_2)^2 + \text{h.c.}\right] - \frac{1}{2}\left\{m_{11}^2(\phi_1^\dagger\phi_1) + \left[m_{12}^2(\phi_1^\dagger\phi_2) + \text{h.c.}\right] + m_{22}^2(\phi_2^\dagger\phi_2)\right\}. \end{aligned} \tag{4.1}$$

The parameters λ_5 and m_{12}^2 are allowed to be complex, subject to the constraint

$$\text{Im}\, m_{12}^2 = \text{Im}\, \lambda_5\, v_1 v_2, \tag{4.2}$$

with v_1 and v_2 the vacuum expectation values ($v_1^2 + v_2^2 = v^2$, with $v = 246$ GeV). It is this quantity, $\text{Im}\, m_{12}^2$ (or $\text{Im}\, \lambda_5$) which leads to CP violation, and one may think of CP

violation as being introduced softly, via the mass term m_{12}^2 in (4.1). Since the potential has a Z_2 symmetry that is only broken softly by the m_{12}^2 term, flavour-changing neutral currents are suppressed [18, 19].

The neutral-sector mass squared matrix corresponding to the potential (4.1) can be written as (for details, see [6])

$$\mathcal{M} = v^2 \begin{pmatrix} \lambda_1 c_\beta^2 + \nu s_\beta^2 & (\lambda_{345} - \nu) c_\beta s_\beta & -\frac{1}{2}\mathrm{Im}\,\lambda_5\, s_\beta \\ (\lambda_{345} - \nu) c_\beta s_\beta & \lambda_2 s_\beta^2 + \nu c_\beta^2 & -\frac{1}{2}\mathrm{Im}\,\lambda_5\, c_\beta \\ -\frac{1}{2}\mathrm{Im}\,\lambda_5\, s_\beta & -\frac{1}{2}\mathrm{Im}\,\lambda_5\, c_\beta & -\mathrm{Re}\;\lambda_5 + \nu \end{pmatrix} \tag{4.3}$$

with the abbreviations $c_\beta = \cos\beta$, $s_\beta = \sin\beta$, $\tan\beta = v_2/v_1$, $\lambda_{345} = \lambda_3 + \lambda_4 + \mathrm{Re}\,\lambda_5$, $\nu = \mathrm{Re}\, m_{12}^2/(2v^2 \sin\beta\cos\beta)$ and $\mu^2 = v^2\nu$.

For $\mathrm{Im}\,\lambda_5 \neq 0$, the elements $\mathcal{M}_{13}$ and $\mathcal{M}_{23}$ provide mixing between the 2×2 upper left part of the matrix and $\mathcal{M}_{33}$. These two sectors would otherwise represent two scalar (usually denoted h and H) and one pseudoscalar Higgs boson (denoted A). We note that these two "mixing elements" are related via $\tan\beta$:

$$\mathcal{M}_{13} = \tan\beta\, \mathcal{M}_{23}. \tag{4.4}$$

It is in this sense that the CP violation is *minimal* in structure. This simple relation is violated in more general models, with so-called λ_6 and λ_7 terms in the potential [6].

We diagonalize (4.3) with the matrix R, defined such that

$$R\mathcal{M}R^{\mathrm{T}} = \mathrm{diag}(M_1^2, M_2^2, M_3^2), \tag{4.5}$$

and use for the rotation matrix [20]

$$\begin{aligned} R = R_c\, R_b\, R_{\tilde{\alpha}} &= \begin{pmatrix} 1 & 0 & 0 \\ 0 & \cos\alpha_c & \sin\alpha_c \\ 0 & -\sin\alpha_c & \cos\alpha_c \end{pmatrix} \begin{pmatrix} \cos\alpha_b & 0 & \sin\alpha_b \\ 0 & 1 & 0 \\ -\sin\alpha_b & 0 & \cos\alpha_b \end{pmatrix} \begin{pmatrix} \cos\tilde{\alpha} & \sin\tilde{\alpha} & 0 \\ -\sin\tilde{\alpha} & \cos\tilde{\alpha} & 0 \\ 0 & 0 & 1 \end{pmatrix} \\ &= \begin{pmatrix} c_{\tilde{\alpha}}\, c_b & s_{\tilde{\alpha}}\, c_b & s_b \\ -(c_{\tilde{\alpha}}\, s_b\, s_c + s_{\tilde{\alpha}}\, c_c) & c_{\tilde{\alpha}}\, c_c - s_{\tilde{\alpha}}\, s_b\, s_c & c_b\, s_c \\ -c_{\tilde{\alpha}}\, s_b\, c_c + s_{\tilde{\alpha}}\, s_c & -(c_{\tilde{\alpha}}\, s_c + s_{\tilde{\alpha}}\, s_b\, c_c) & c_b\, c_c \end{pmatrix} \end{aligned} \tag{4.6}$$

with $c_i = \cos\alpha_i$, $s_i = \sin\alpha_i$. The angular range, beyond which R is repeated, can be chosen as $-\pi/2 < \tilde{\alpha} \leq \pi/2$, $-\pi < \alpha_b \leq \pi$, and $-\pi/2 < \alpha_c \leq \pi/2$. However, the physical range is more restricted, since we require $M_1 \leq M_2 \leq M_3$.

There are certain symmetries, under which the masses are unchanged, but one or two rows of R (i.e., physical Higgs fields) change sign. These symmetries are:

$$\begin{aligned} &\text{A}: \quad \tilde{\alpha} \text{ fixed},\ \alpha_c \to -\alpha_c,\ \alpha_b \to \pi + \alpha_b: \quad R_{1i} \to -R_{1i}, \quad R_{2i} \to R_{2i}, \quad R_{3i} \to -R_{3i}, \\ &\text{B}: \quad \tilde{\alpha} \to \pi + \tilde{\alpha},\ \alpha_b \to -\alpha_b,\ \alpha_c \to -\alpha_c: \quad R_{1i} \to -R_{1i}, \quad R_{2i} \to -R_{2i}, \quad R_{3i} \to R_{3i}. \end{aligned} \tag{4.7}$$

In addition, we have the following symmetry for $\tilde{\alpha}$, α_c fixed:

$$\text{C}: \quad \alpha_b \to \pi - \alpha_b,\ \alpha_b > 0\ (\alpha_b \to -\pi - \alpha_b,\ \alpha_b < 0): \quad R_{1i} \to -R_{1i}, \quad R_{j3} \to -R_{j3}, \tag{4.8}$$

the other elements in R being unchanged. Finally, we have, for α_b, α_c fixed:

$$\text{D}: \quad \tilde{\alpha} \to \pi + \tilde{\alpha}: \quad R_{j1} \to -R_{j1}, \quad R_{j2} \to -R_{j2}, \quad R_{j3} \to R_{j3}. \tag{4.9}$$

(The symmetries B and D are of marginal interest, since they only relate the *edges* of the angular range.)

The CP-conserving case is obtained by taking $\alpha_b = 0$ or $\alpha_b = \pi$, together with $\alpha_c = 0$ and $\tilde{\alpha} = \frac{1}{2}\pi + \alpha$ arbitrary. Here, α is the familiar mixing angle of the CP-even sector. Thus, as alternatives to $\mathrm{Im}\,\lambda_5$, the angles α_b and α_c parametrize the mixing that leads to CP violation. Of course, replacing one parameter by two, constraints are imposed on the mass spectrum.

Yukawa couplings

With this notation, and adopting the so-called Model II [21] for the Yukawa couplings, where the down-type and up-type quarks are coupled only to ϕ_1 and ϕ_2, respectively, the $Ht\bar{t}$ couplings can be expressed (relative to the SM coupling) as

$$H_j t\bar{t}: \qquad \frac{1}{\sin\beta}\left[R_{j2} - i\gamma_5 \cos\beta R_{j3}\right] \equiv a + i\tilde{a}\gamma_5. \tag{4.10}$$

As mentioned in the Introduction, the product of the scalar and pseudoscalar couplings,

$$\gamma_{CP} = -a\,\tilde{a} = \frac{\cos\beta}{\sin^2\beta} R_{j2} R_{j3} \tag{4.11}$$

plays an important role in determining the amount of CP violation. We note the following symmetries of γ_{CP} for any of the three Higgs bosons H_j $(j = 1, 2, 3)$:

- under the symmetries "A" and "B" of (4.7), γ_{CP} is invariant,
- under the symmetries "C" and "D", γ_{CP} changes sign.

As was seen in sect. 3, unless the Higgs boson is resonant with the $t\bar{t}$ system, CP violation is largest for small Higgs masses. We shall therefore focus on the contributions of the lightest Higgs boson, H_1. For the lightest Higgs boson, the coupling (4.10) becomes

$$H_1 t\bar{t}: \qquad \frac{1}{\sin\beta}\left[\sin\tilde{\alpha}\cos(\alpha_b) - i\gamma_5\cos\beta\sin(\alpha_b)\right], \quad \text{with} \quad \gamma_{CP} = \tfrac{1}{2}\frac{\sin\tilde{\alpha}\sin(2\alpha_b)}{\tan\beta\sin\beta}, \tag{4.12}$$

where $\tilde{\alpha}$ and α_b are mixing angles of the Higgs mass matrix as defined above.

When the three neutral Higgs bosons are light, they will *all* contribute to the CP-violating effects. In fact, in the limit of three mass-degenerate Higgs bosons, the CP violation will cancel, since [cf. eq. (4.11)]

$$\sum_{j=1}^{3}\gamma_{CP} = \frac{\cos\beta}{\sin^2\beta}\sum_{j=1}^{3}R_{j2}\,R_{j3} = 0 \tag{4.13}$$

due to the orthogonality of R.

"Maximal CP violation"

The $|\gamma_{CP}|$ of eq. (4.12) is readily maximized w.r.t. the rotation angles $\tilde{\alpha}$ and α_b:

$$\tilde{\alpha}^{\max CP} = \pm\tfrac{1}{2}\pi, \quad \alpha_b^{\max CP} = \pm\tfrac{1}{4}\pi \ \text{ or } \ \pm\tfrac{3}{4}\pi, \tag{4.14}$$

whereas it increases with *decreasing* values of $\tan\beta$. Negative values of α_c are related to positive values through the symmetry "A" of eq. (4.7) and need not be considered separately. Similarly, the case of $\alpha_b = 3\pi/4$ is related to that of $\alpha_b = \pi/4$ by the symmetry "C" and just leads to an over-all change of sign for γ_{CP}. We shall somewhat imprecisely (since also H_2 and H_3 contribute) refer to these cases (4.14) as "maximal CP violation".

More generally, large CP-violating effects are expected when $|\mathrm{Im}\,\lambda_5|$ is large, or, when the elements $\mathcal{M}_{13}$ and $\mathcal{M}_{23}$ are large, see (4.3). These can be expressed in terms of the rotation matrix and the mass eigenvalues as

$$\mathcal{M}_{13} = R_{11}R_{13}M_1^2 + R_{21}R_{23}M_2^2 + R_{31}R_{33}M_3^2,$$

$$\mathcal{M}_{23} = R_{12}R_{13}M_1^2 + R_{22}R_{23}M_2^2 + R_{32}R_{33}M_3^2. \tag{4.15}$$

In this description, one measure of "maximal mixing" would be to ignore the lightest mass, and then require the coefficients of M_2^2 and M_3^2 to be equal in magnitude. This would require $|\sin(\tilde{\alpha})| = 0$ or $|\cos(\tilde{\alpha})| = 0$, i.e., $\tilde{\alpha} = 0$, $\pm\frac{1}{2}\pi$ or π, and simultaneously $|\sin(2\alpha_b)| = |\sin(2\alpha_c)| = 1$. We shall refer to these cases as "maximal mixing".

The bounds on the electric dipole moments of the neutron and the electron impose restrictions on the allowed magnitude of CP violation in the 2HDM. We note that, within a consistent framework, and for maximal CP violation in the Higgs–gauge sector [22] (which amounts to maximizing the product of the three couplings (4.26), and thus is different from the present concept of "maximal CP violation", where we consider Yukawa interactions only), those bounds restrict the mass splitting between M_2 and M_3 to be less than $\mathcal{O}(15\% - 20\%)$ [23].

4.2 Physical content

Specifying all the parameters of the potential, as well as the structure of the Yukawa couplings, the physical content of the model is fixed. We shall here follow a somewhat different approach: We start out by specifying the masses of two Higgs bosons (the lightest and one other), together with $\tan\beta$ and the three angles that determine R. Then, unless $\alpha_b = 0$ or $\alpha_c = 0$, the third Higgs mass can be determined, as well as all the couplings. This approach gives more "control" of the physical input.

With $\tan\beta$, R and the masses of *two* neutral Higgs bosons fixed, the third one is given by

$$R_{13}(R_{11} - R_{12}\tan\beta)M_1^2 + R_{23}(R_{21} - R_{22}\tan\beta)M_2^2 + R_{33}(R_{31} - R_{32}\tan\beta)M_3^2 = 0, \tag{4.16}$$

where we have assumed $\mathrm{Im}\,\lambda_5 \neq 0$ and made use of the relation (4.4). Invoking the orthogonality of R, one sees that this relation (4.16) only relates *differences* of masses squared:

$$R_{23}(R_{21} - R_{22}\tan\beta)(M_2^2 - M_1^2) + R_{33}(R_{31} - R_{32}\tan\beta)(M_3^2 - M_1^2) = 0. \tag{4.17}$$

In general, as two Higgs masses approach each other, also the third mass has to approach the same value, as we can read off eq. (4.17). However, for particular choices of the

parameters, this is not the case. For example, if we put the coefficient of M_1^2 in eq. (4.16) equal to zero, one has $M_2 = M_3$ for

$$R_{13}(R_{11} - R_{12}\tan\beta) = 0. \tag{4.18}$$

This equation is satisfied for *(i)* $R_{13} = 0$, or *(ii)* $\tan\beta = R_{11}/R_{12}$ or *(iii)* R_{11} and R_{12} each zero. Solution *(i)* implies $\alpha_b = 0$, whereas solution *(ii)* implies $\tan\beta = \cot\tilde{\alpha}$, or $\tilde{\alpha} = \frac{1}{2}\pi - \beta$. Solution *(iii)* implies $|\alpha_b| = \pi/2$ where, non-interestingly, the three masses are arbitrarily chosen. Following from *(ii)*, for example, we get $M_2 = M_3$ for arbitrary M_1, for the choice of parameters $\tan\beta = 1$ and $\tilde{\alpha} = \pi/4$.

Allowed regions in the parameter space

In fig. 7 we show the allowed regions in the α_b–α_c plane for selected values of $\tan\beta$ and $\tilde{\alpha}$, subject to the constraint $M_1 \leq M_2 \leq M_3$. Regions of negative α_c and $|\alpha_b| > \pi/2$ are not shown, they follow by the symmetries "A" and "C", respectively, of eq. (4.7).

In this analysis, we keep M_1 and M_2 fixed, and determine M_3 from eq. (4.16). Clearly, this breaks down when

$$R_{33}(R_{31} - R_{32}\tan\beta) = 0, \tag{4.19}$$

in which case M_3 is not determined. This occurs deep inside the unphysical region, as explained below.

The dark (blue) regions in fig. 7 are allowed, the white ones are not allowed. Some reasons why a region is physically forbidden are: (*i*) the equation for M_3 has no solution (for example, when $M_3^2 < 0$, or when eq. (4.19) holds), (*ii*) $M_3 > M_2$ is violated, (*iii*) positivity of the potential (4.1) is violated, or (*iv*) perturbativity is violated. The requirement to perturbativity is taken as

$$|\lambda_i| < 4\pi\xi, \tag{4.20}$$

where we somewhat arbitrarily take $\xi = 0.8$. The lightly shaded (yellow) regions are also allowed, if we use a less stringent condition on perturbativity, $\xi = 1.0$.[7] The cut-off against

[7] These numbers are of course only order-of-magnitude indicators. For example, one could argue that since λ_1 and λ_2 are accompanied by factors 1/2 in the potential (and hence in all couplings), the relevant limit is 8π, not 4π.

the disallowed region depends on the additional parameters, which we in this figure take as $M_1 = 100$ GeV, $M_2 = 300$ GeV, $M_{H^\pm} = 500$ GeV, and $\mu = 0$ (corresponding to Case I, studied in sect. 5.1). This dependence enters via the conversion of the masses of the neutral Higgs bosons, and the rotation angles, to λ's.

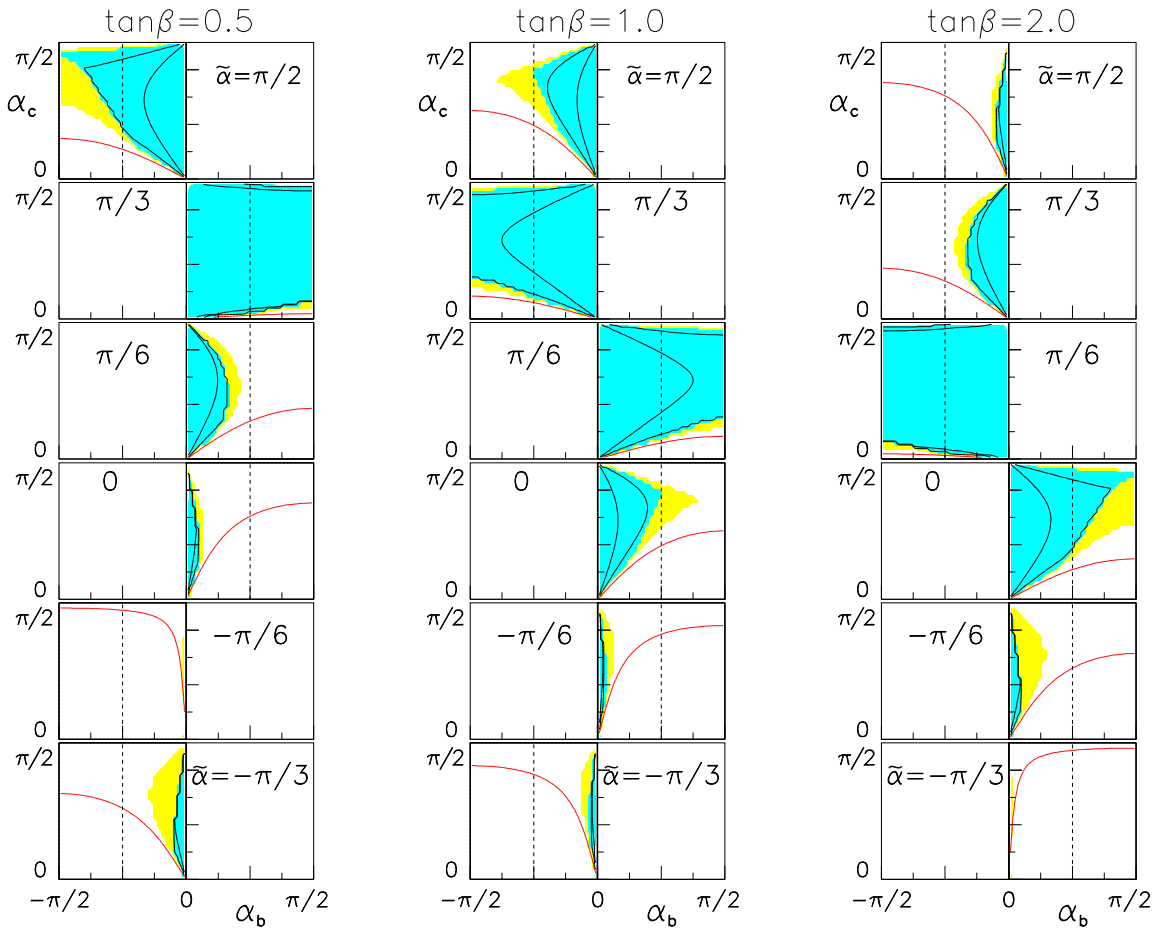

Figure 7: Physically allowed regions in the α_b–α_c plane, for $\tan\beta = 0.5$, 1 and 2 and for selected values of $\tilde{\alpha}$. Blue (dark): allowed regions; white: not allowed; yellow: marginally allowed (see text). The dashed lines at $\alpha_b = \pm\pi/4$ are lines of "maximum CP violation". Solid contours in allowed regions: $M_2/M_3 = 0.6$ and 0.8 ($M_2 = M_3$ along $\alpha_b = 0$). For no choice of mass parameters can the allowed region extend beyond the solid contours in the forbidden region.

The condition (4.19), which is satisfied for

$$(1) \quad R_{33} = 0, \qquad \text{or} \quad (2) \quad R_{31} - R_{32}\tan\beta = 0, \tag{4.21}$$

defines borders where M_3^2 changes sign. We note that *these borders are independent of the mass parameters of the model*. Thus, they are absolute borders which the physically allowed region can never cross for any choice of mass parameters. Let us now discuss the two cases of eq. (4.21). In the α_b–α_c plane, case (1) is satisfied when $\cos\alpha_b = 0$ or when $\cos\alpha_c = 0$. When $\cos\alpha_b = 0$, then eq. (4.16) is trivially satisfied, so this is not interesting. The second subcase, $\cos\alpha_c = 0$, corresponds to the upper boundary of the plots in fig. 7, $\alpha_c = \pi/2$. Since this line represents a border where M_3^2 changes from $+\infty$ to $-\infty$, there is a region next to it where M_3 is so large that perturbativity breaks down (and hence forbidden), as indeed seen in the figure.

Coming now to the more interesting case (2) of (4.21), which, according to eq. (4.6) is satisfied for

$$\tan(\beta+\tilde{\alpha})\,\tan\alpha_c = \sin\alpha_b, \tag{4.22}$$

we obtain the contours shown in fig. 7 deep inside the unphysical region.

These contours must be in the same "quadrant" in the α_b–α_c plane as where the physically allowed region is located. This can be seen as follows. On one side of the contour, M_3^2 is large and positive. By continuity, moving from the contour toward the line $\alpha_b = 0$, where $M_3 = M_2$, the value of M_3 will inevitably pass through an allowed region where $M_3 \gtrsim \mathcal{O}(M_2)$.

This observation allows us to determine in which quadrant the physically allowed regions are located. Near the origin, (4.22) can be approximated as

$$\tan(\beta+\tilde{\alpha}) \simeq \frac{\alpha_b}{\alpha_c}. \tag{4.23}$$

Thus, $\alpha_b\alpha_c > 0$ when

$$0 < \beta+\tilde{\alpha} < \tfrac{1}{2}\pi, \qquad \text{First (or third) quadrant} \tag{4.24}$$

whereas $\alpha_b\alpha_c < 0$ when

$$-\tfrac{1}{2}\pi < \beta+\tilde{\alpha} < 0 \quad \text{or} \quad \tfrac{1}{2}\pi < \beta+\tilde{\alpha} < \pi, \qquad \text{Second (or fourth) quadrant} \tag{4.25}$$

in agreement with fig. 7. Finally, we note from (4.23) that the physical region may occupy a large fraction of the actual quadrant when $|\beta+\tilde{\alpha}| \simeq \pi/2$, and only a small fraction of the quadrant when $|\beta+\tilde{\alpha}| \simeq 0$ or π.

Higgs–vector–vector couplings

The non-discovery of a Higgs boson at LEP poses constraints on $\tan\beta$ and on the Higgs mass. While SM Higgs masses below 115 GeV are excluded [24], as well as $\tan\beta \lesssim 2$–3 in the MSSM [25], these bounds can be eluded in the 2HDM, if the lightest Higgs boson couples with sufficiently reduced strength to the vector bosons. In fact, this coupling is (relative to the corresponding SM coupling) given by

$$H_i ZZ : \qquad \cos\beta\, R_{i1} + \sin\beta\, R_{i2}. \tag{4.26}$$

Higgs masses down to about 50 GeV are allowed, provided this coupling squared is less than about 0.5 [26].

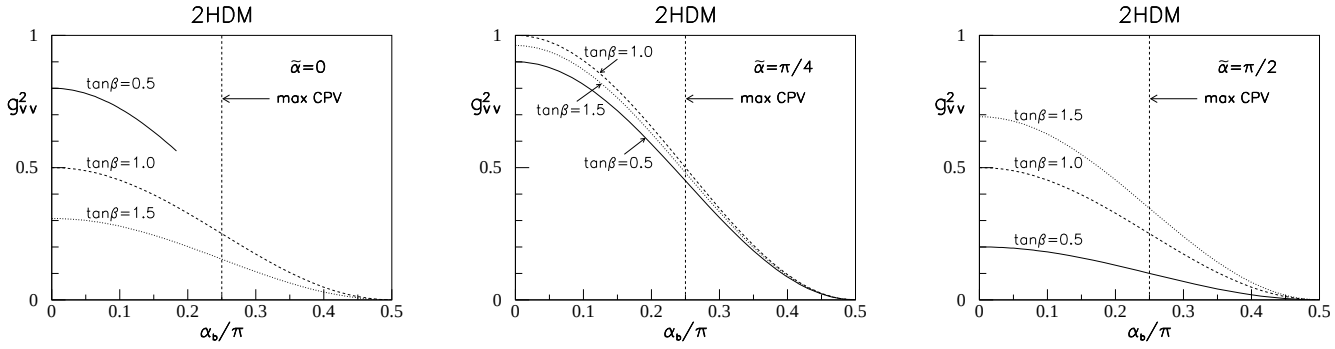

Figure 8: Squared coupling of the *lightest* Higgs boson to vector bosons (relative to that of the Standard Model), g^2_{VV}, *vs.* mixing angle α_b, for fixed $\tilde\alpha = 0$, $\pi/4$ and $\pi/2$. These couplings are symmetric under $\alpha_b \to \pi - \alpha_b$, and independent of α_c. For $\tilde\alpha = 0$ and $\tan\beta = 0.5$, only small values of α_b are allowed for the chosen mass parameters: $M_1 = 100$ GeV, $M_2 = 300$ GeV, $M_{H^\pm} = 500$ GeV, $\alpha_c = \pi/3$ and $\xi = 0.8$ (cf. fig. 7).

We show in fig. 8 the square of the coupling of the lightest Higgs boson to vector bosons, relative to that of the Standard Model, g^2_{VV}, for low values of $\tan\beta$. As discussed above, for masses of the lightest Higgs below ~ 100 GeV, this quantity should be well below unity, in order not to be in conflict with the non-observation of a Higgs boson at LEP2 [24].

It should be noted that this coupling can be expressed in terms of angles only, without any dependence on masses. However, for certain combinations of mass parameters and α_c

values, some α_b ranges might be unphysical, as illustrated for $\tilde{\alpha} = 0$ and $\tan\beta = 0.5$ in this figure, as well as in fig. 7.

5 Case Studies

In order to get a better idea how much CP violation the 2HDM can give, we shall here discuss the case of "maximal CP violation" in the sense of eq. (4.14), together with small values of $\tan\beta$ and light Higgs masses.

In the following two subsections, we shall analyze two cases, first (sec. 5.1) the case of two Higgs bosons being light, and then (sec. 5.2) the case of one light and two heavy ones. These are qualitatively different, since in the first case there will be considerable cancellations among the CP-violating contributions, because of (4.13).

With all mixing angles fixed, and two Higgs masses specified, the third Higgs mass is determined. Thus, the "soft" mass term $\mu^2 = \mathrm{Re}\, m_{12}^2 / \sin 2\beta$ only enters in converting the masses (and angles) to λ's. We check that the required λ's satisfy positivity of the potential and perturbativity, eq. (4.20).

5.1 Case 1. Two light and one heavy Higgs bosons

As a first case, we consider $M_1 \leq M_2 = 300$ GeV (below the $t\bar{t}$ threshold) with $M_{H^\pm} = 500$ GeV and $\tan\beta = 0.5$ and 1.0. (This is well within the limits on $M_{H^\pm}$ and $\tan\beta$ derived from studies of meson decays and mixings [27].) Then, for $\alpha_c = \pi/4$, $\pi/3$ and $5\pi/12$, we show in fig. 9 the heaviest Higgs boson mass, M_3 *vs.* M_1, for $\tan\beta = 0.5$, 1.0 and 1.5. We note that, for some of the parameters considered, there is no solution (we take $\xi = 1.0$), as also follows from fig. 7.

In fig. 10 we show, for this case of "maximal CP violation" and low values of $\tan\beta$ ($\tan\beta = 0.5$ and 1.0), the corresponding signal-to-noise ratio of the observable A_1 (3.4), for M_1 ranging from 80 to 300 GeV, keeping $M_2 = 300$ GeV fixed and letting M_3 vary accordingly. We show separately the contributions of only the lightest Higgs boson, and the contributions of all three. Considering only the contribution of the lightest Higgs boson, the CP-violating effects are seen to be significantly larger than in the "general case" studied

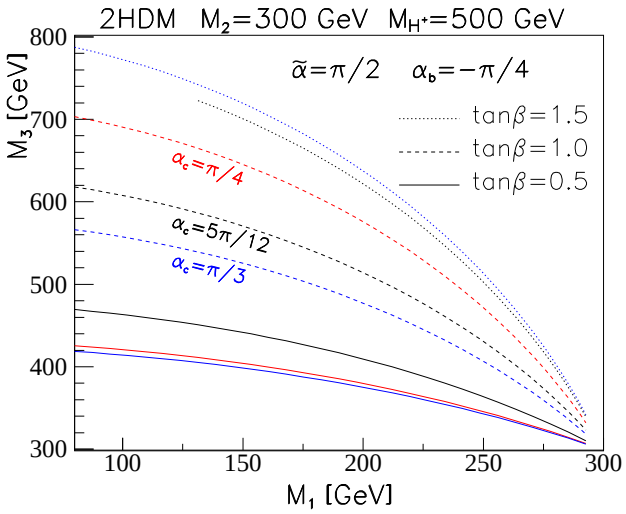

Figure 9: Heaviest Higgs-boson mass, M_3 *vs.* M_1, for $M_2 = 300$ GeV, and $M_{H^\pm} = 500$ GeV, for three values of $\alpha_c = \pi/4$, $\pi/3$ and $5\pi/12$, and three values of $\tan\beta = 0.5$, 1.0 and 1.5. Furthermore, we consider "maximal CP violation" with $\tilde{\alpha} = \pi/2$ and $\alpha_b = -\pi/4$.

in sect. 3, essentially because of the enhancement of γ_{CP} due to the small values of $\tan\beta$. We note that, for the parameters considered here ($\tilde{\alpha} = \pi/2$ and $\alpha_b = -\pi/4$), and for the lightest Higgs boson, γ_{CP} is negative, contrary to the case studied in sect. 3.

However, in the present case, the inclusion of all three contributions leads to large cancellations. This also implies that, even if no CP violation should be observed, it may be difficult to conclude that the Higgs sector conserves CP, since such cancellations are possible.

As expected, the CP-violating effects are largest for low values of M_1. Since the two lightest Higgs bosons are below the $t\bar{t}$ resonance, there is a smooth dependence on M_1. As M_1 approaches M_2 (where all three masses are degenerate), the CP-violating effects cancel. On the whole, the resulting CP violation is reduced by a factor of $\sim 1/4$ compared to the "model-independent" case considered in sect. 3.

Whereas the top Yukawa couplings of the *lightest* Higgs boson do not depend on α_c, some dependence on this quantity enters, via the couplings of the two heavier Higgs bosons to the t quark. This is also illustrated in fig. 10.

Since the two heavier Higgs bosons can contribute significantly to $\langle A_1 \rangle$, the dependence

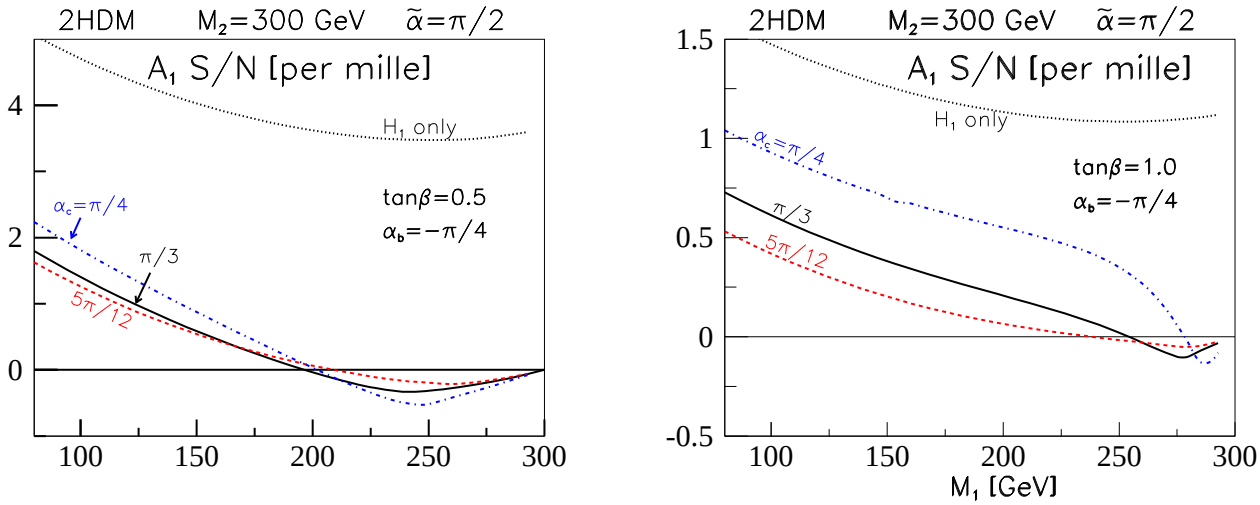

Figure 10: Signal-to-noise ratio, for lepton energy correlations $\langle A_1 \rangle$ in $pp \to t\bar{t}X$ *vs.* lightest Higgs mass for the 2HDM, for a case of three moderately light Higgs bosons (see fig. 9) and $\tan\beta = 0.5$ and 1.0. "Maximal CP violation" is considered (cf. eq. (4.14)), and $\alpha_c = \pi/4$, $\pi/3$ and $5\pi/12$. Also shown, is the contribution of the lightest Higgs boson only (independent of α_c).

on α_b need not be as simple as discussed in sect. 4.1. In particular, the CP violation need not be maximal for $\alpha_b = \pm\pi/4$ (or $\pm 3\pi/4$). Fig. 11 (left panel) illustrates the dependence on α_b for fixed $\tilde{\alpha} = \pi/2$, $\alpha_c = \pi/3$, and two values of $\tan\beta$ (0.5 and 1.0). One confirms the general impression from the form of (4.6) and the discussion following (4.15), that $|\alpha_b|$ should be sizable, but not necessarily $\pi/4$, in order to maximize the CP violation.

It is also possible that one Higgs boson does not violate CP in its couplings to the t quark, and yet the other two do. For example, for $\tilde{\alpha} = 0$, the lightest Higgs boson has a pure pseudoscalar coupling to the top quark, and hence the CP violation is exclusively due to the two heavier Higgs bosons. In this case, the resulting total contribution to the lepton energy correlations $\langle A_1 \rangle$ may even exceed that obtained when the contribution of the lightest Higgs boson is maximal, see fig. 11 (right panel).

5.2 Case 2. One light and two heavy neutral Higgs bosons

Next, we let two of the neutral Higgs boson masses be more heavy, taking $M_3 \geq M_2 = 500$ GeV, and $M_{H^\pm} = 700$ GeV. The resulting mass values, M_3, are shown in fig. 12, for

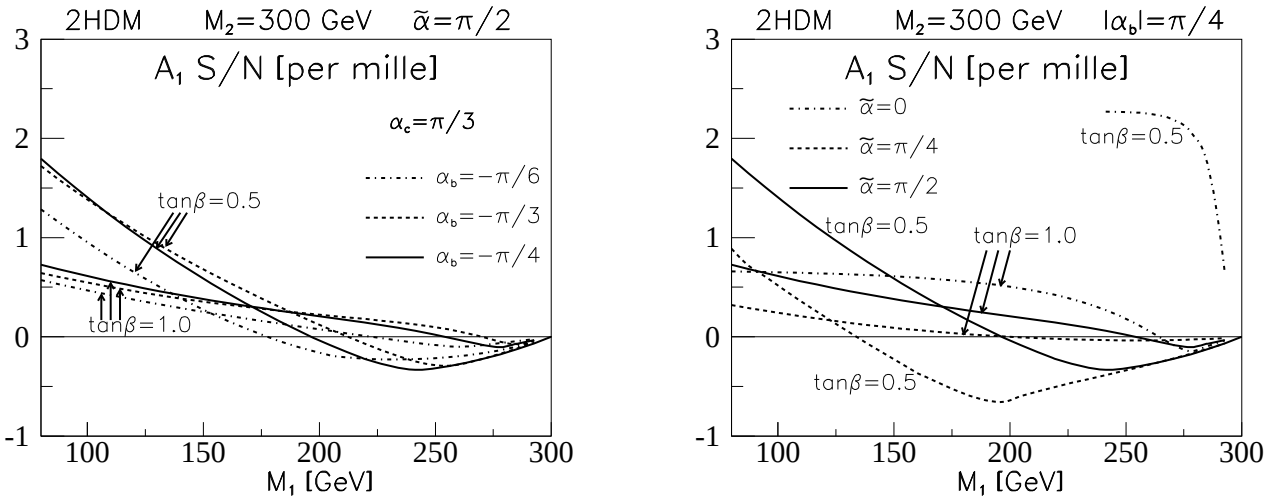

Figure 11: Sensitivity of A_1 in $pp \to t\bar{t}X$ *vs.* lightest Higgs mass. *Left panel:* Different values of α_b are studied, for fixed $\tilde{\alpha} = \pi/2$, $\alpha_c = \pi/3$. *Right panel:* Different values of $\tilde{\alpha}$ are studied, $\tilde{\alpha} = 0$, $\pi/4$ and $\pi/2$ ("maximal mixing") with $\alpha_c = \pi/3$ (see fig. 7). The mixing angle $|\alpha_b| = \pi/4$ is kept fixed. Two values of $\tan\beta$ are considered: 0.5 and 1.0.

two values of $\tilde{\alpha}$, three values of $\alpha_c = \pi/4$, $\pi/3$ and $5\pi/12$, and small values of $\tan\beta$. For the cases studied in sect. 5.1, solutions could be found with $\mu = 0$. This is here not the case. For $\tilde{\alpha} = \pi/2$ ("maximal CP violation"), *no* value of μ allows a light H_1 (fig. 12, right panel), so we have included also $\tilde{\alpha} = \pi/3$ (left panel), where light H_1 can be realized for large μ.

We show in fig. 13 the corresponding results for the lepton energy asymmetry, $\langle A_1 \rangle$, for $\tan\beta = 0.5$ and 1. In this case, as opposed to the cases considered in sect. 5.1, since H_2 and H_3 are heavier, it is a good approximation to consider only H_1 exchange up to $M_1 \sim 450$ GeV. As a result, the CP-violating effects are significantly larger than in the low-mass case studied in sect. 5.1. The amount of CP-violation for *one* light Higgs boson, $M_1 = \mathcal{O}(100$ GeV), is comparable with, and may exceed that obtained for a mass around the $t\bar{t}$ resonance.

We note that there is only a rather weak dependence on α_c. This is clearly due to the fact that the contribution of H_1 (which is independent of α_c) dominates. (However, as $\alpha_c \to 0$, the physical range of M_1 shrinks, cf. fig. 7.)

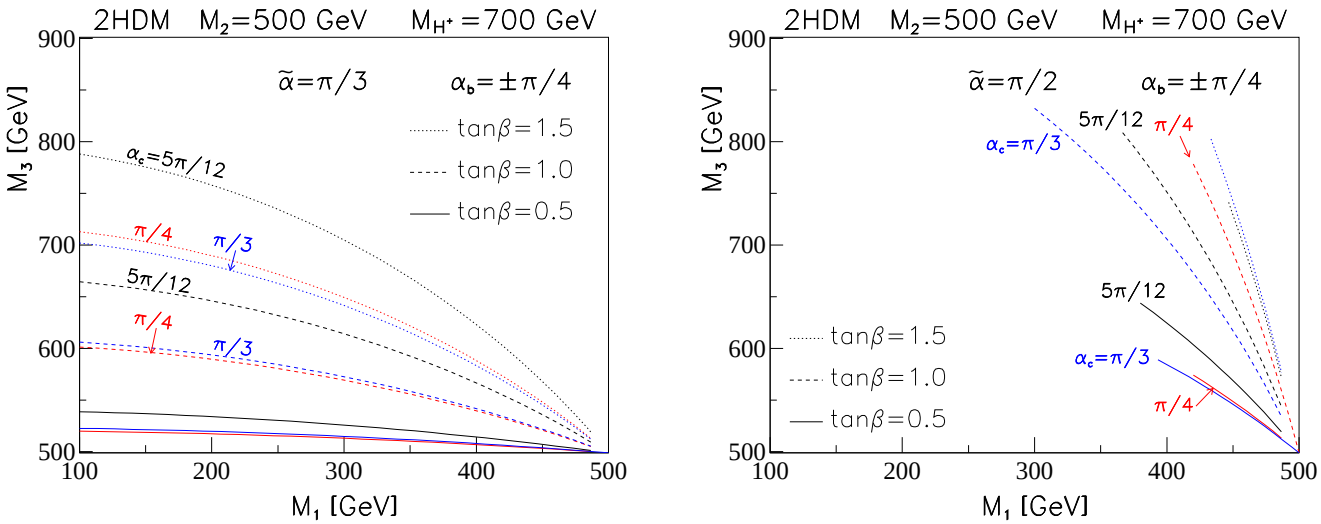

Figure 12: Heaviest Higgs-boson mass, M_3 *vs.* M_1, for $M_2 = 500$ GeV and $M_{H^\pm} = 700$ GeV. For some parameters, there is a lower limit for M_1, due to perturbativity, eq. (4.20), where we take $\xi = 1.0$.

Fig. 14 is devoted to a study of the dependence of α_b. As expected (since H_1 dominates), the CP violation is maximized for $\alpha_b \simeq -\pi/4$. As $\alpha_b \to 0$, the effect vanishes. There are in fact two reasons for this. First, the contribution of H_1 to γ_{CP} vanishes linearly. Secondly, M_2 and M_3 become degenerate in this limit. According to the discussion in sect. 4.2, all three masses must then become degenerate, and there is no CP violation.

5.3 Case 3. The $t\bar{t}$ transition region

As is seen from fig. 4, and also from a qualitative comparison of Case 1 and Case 2, there is in general less CP-violation if two Higgs masses are below the $t\bar{t}$ threshold than if two masses are above. We here explore this transition region in a little more detail, by comparing in fig. 15 a few values of *the intermediate Higgs boson mass* M_2, below and above the $t\bar{t}$ threshold, keeping the mixing angles fixed at $\tilde{\alpha} = \pi/2$, $\alpha_b = -\pi/4$, $\alpha_c = \pi/3$ and $\tan\beta = 0.5$. One sees that, for values of M_1 well below M_2, there is little dependence on M_2, unless M_2 is *above* the $t\bar{t}$ threshold, in which case the CP-violation (for fixed M_1) increases rapidly with M_2.

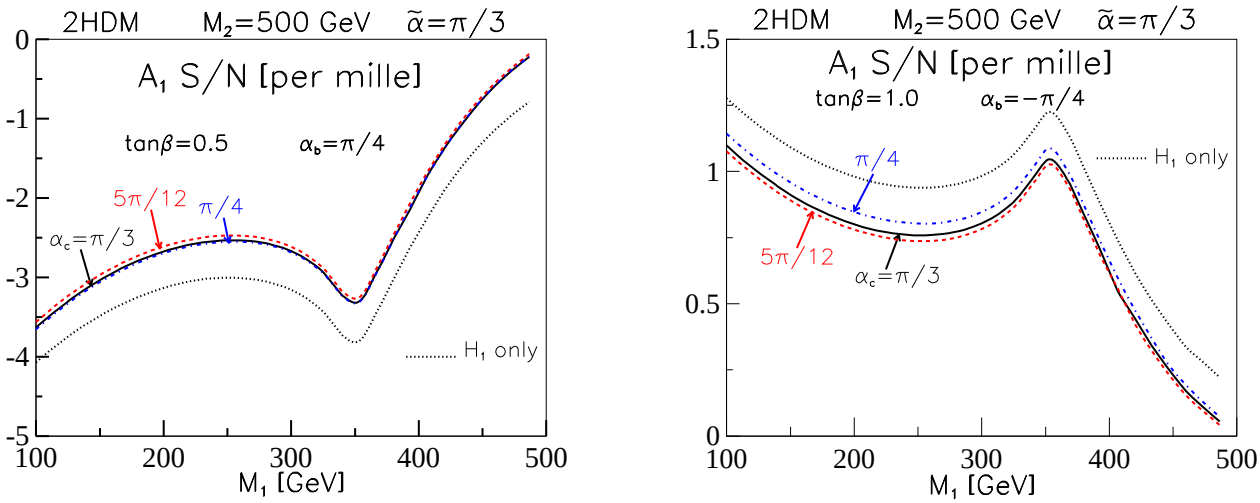

Figure 13: Signal-to-noise ratio, for lepton energy correlations $\langle A_1 \rangle$ in $pp \to t\bar{t}X$ *vs.* Higgs mass for the 2HDM. Similar to fig. 10 for $\tilde{\alpha} = \pi/3$ and $M_3 > M_2 = 500$ GeV, with $M_{H^\pm} = 700$ GeV. Note that one set of curves is "upside–down" with respect to the other, since the α_b-values have opposite signs (we keep α_c positive in both cases).

6 Concluding remarks

We have reviewed and confirmed the basic results of [3] on CP violation induced by non-standard Higgs exchange in the production of $t\bar{t}$ pairs at the LHC, up to a few misprints. The results for the box diagram have been further reduced to basic loop integrals. Some modifications of their observable $A_1 = E_+ - E_-$ (where $E_\pm$ are the lepton energies) have been investigated. These modifications can in some kinematical situations improve the signal-to-noise ratio, provided the $t\bar{t}$ invariant mass can be determined with a reasonable precision.

For the observable $A_2 = \mathbf{p}_{\bar{t}} \cdot \mathbf{l}^+ - \mathbf{p}_t \cdot \mathbf{l}^-$, we find a much lower signal-to-noise ratio than was given in [3]. This observable thus appears less suited for a search for CP violation at the LHC (for details, see sect. 3.2).

In a minimal, CP-violating Two-Higgs-Doublet Model, where couplings and masses are constrained and related by the Higgs potential and the Yukawa couplings ("Model II"), the CP-violating effects can at the LHC be at the per mille level, as given by Bernreuther and Brandenburg [3] (see also [1]), provided that (i) $\tan\beta$ is small ($\lesssim 1$), and that (ii) there is

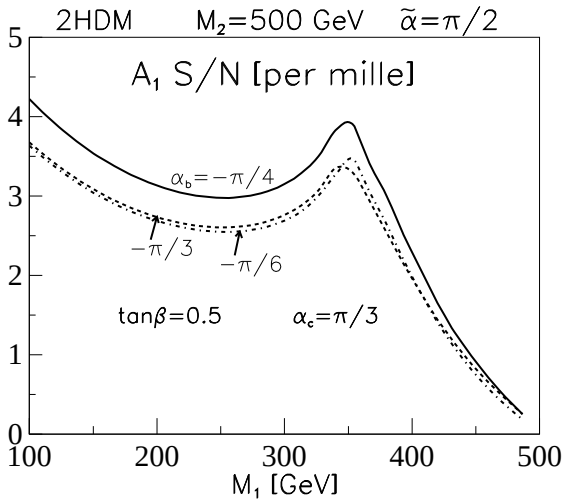

Figure 14: Signal-to-noise ratio, for lepton energy correlations $\langle A_1 \rangle$ in $pp \to t\bar{t}X$ *vs.* Higgs mass for the 2HDM. Similar to fig. 13 for three values of α_b.

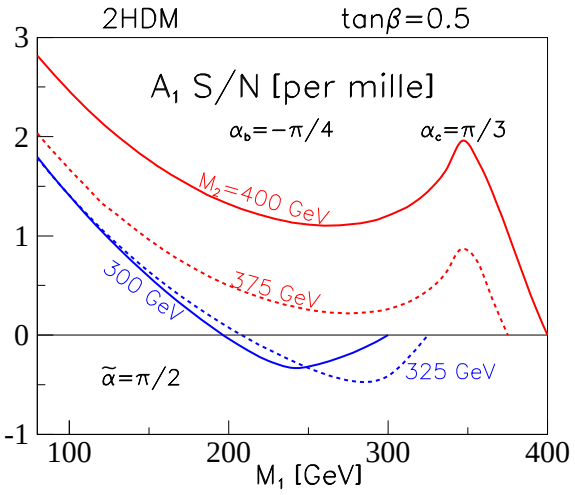

Figure 15: Lepton energy correlations $\langle A_1 \rangle$ in $pp \to t\bar{t}X$ *vs.* Higgs mass for the 2HDM. The intermediate Higgs mass, M_2, is in the $t\bar{t}$ threshold region.

only one light Higgs boson. If there are two neutral Higgs bosons below the $t\bar{t}$ threshold, the effects are severely reduced by cancellations among different contributions.

Our study does not include QCD corrections. Within pure QCD (no Higgs exchange), next-to-leading-order corrections are known [28]. They are not known for these CP-

violating effects. Since we study ratios, one may hope that the dominant parts of the QCD corrections cancel, but this remains to be seen.

Finally, we recall that there are other observables that we have not studied (see, e.g. [4, 29]). At the parton level, the basic asymmetries are larger, of the order of 10^{-2}, as compared with the order 10^{-3} effects discussed here. Thus, for some other choice of observable, it is quite possible that a larger fraction of the 2HDM parameter space could be explored.

Acknowledgments. We would like to thank P.N. Pandita and J. Sjölin for collaboration in early stages of this work. It is also a great pleasure to thank W. Bernreuther and, in particular, A. Brandenburg, for very useful discussions and correspondence. Also, we would like to thank I.F. Ginzburg and M. Krawczyk for discussions on the 2HDM, and W. Hollik and M. Klasen for advice on the "LoopTools" package. This research has been supported by the Research Council of Norway.

Appendix A

In this appendix we collect complete results for the functions b_{g1}^{CP}, b_{g2}^{CP}, c_{g1}, c_{g2} of eq. (2.6), correcting some misprints in [3] and also reducing completely the contribution from the box diagram to four-, three-, and two-point scalar integrals. We define the following two-point functions:

$$B_0(m_t^2, m_H^2, m_t^2) = \frac{1}{i\pi^2}\int d^nq \frac{1}{[(q-\frac{1}{2}Q)^2 - m_t^2][(q-\frac{1}{2}P_t)^2 - m_H^2]}, \tag{A.1}$$

$$B_0(\hat{s}, m_t^2, m_t^2) = \frac{1}{i\pi^2}\int d^nq \frac{1}{[(q+\frac{1}{2}Q)^2 - m_t^2][(q-\frac{1}{2}Q)^2 - m_t^2]}, \tag{A.2}$$

$$B_0(\hat{t}, m_H^2, m_t^2) = \frac{1}{i\pi^2}\int d^nq \frac{1}{[(q-\frac{1}{2}P_g)^2 - m_t^2][(q-\frac{1}{2}P_t)^2 - m_H^2]}, \tag{A.3}$$

three-point functions:

$$C_0(\hat{s}, m_t^2, m_t^2, m_t^2) = \frac{1}{i\pi^2}\int d^nq \frac{1}{[(q+\frac{1}{2}Q)^2 - m_t^2][(q-\frac{1}{2}P_g)^2 - m_t^2][(q-\frac{1}{2}Q)^2 - m_t^2]}, \tag{A.4}$$

$$C_0(\hat{s}, m_H^2, m_t^2, m_t^2) = \frac{1}{i\pi^2}\int d^nq \frac{1}{[(q+\frac{1}{2}Q)^2 - m_t^2][(q-\frac{1}{2}Q)^2 - m_t^2][(q-\frac{1}{2}P_t)^2 - m_H^2]}, \tag{A.5}$$

$$C_0(\hat{t}, m_H^2, m_t^2, m_t^2) = \frac{1}{i\pi^2}\int d^nq \frac{1}{[(q-\frac{1}{2}P_g)^2 - m_t^2][(q-\frac{1}{2}Q)^2 - m_t^2][(q-\frac{1}{2}P_t)^2 - m_H^2]}, \tag{A.6}$$

and the basic four-point function:

$$D_0(\hat{t}) = \frac{1}{i\pi^2}\int d^nq \frac{1}{[(q+\frac{1}{2}Q)^2 - m_t^2][(q-\frac{1}{2}P_g)^2 - m_t^2][(q-\frac{1}{2}Q)^2 - m_t^2][(q-\frac{1}{2}P_t)^2 - m_H^2]}. \tag{A.7}$$

Here, $\hat{s} = Q^2$, $\hat{t} = -Q^2(1-\beta z)$. Furthermore, for $\hat{u} = -Q^2(1+\beta z)$, the scalar integrals $B_0(\hat{u}, m_H^2, m_t^2)$, $C_0(\hat{u}, m_H^2, m_t^2, m_t^2)$ and $D_0(\hat{u})$ are obtained from (A.3), (A.6) and (A.7), respectively, with $P_g \to -P_g$ (or $P_t \to -P_t$). Note that, in this notation of [3], the function $C_0(\hat{s}, m_t^2, m_t^2, m_t^2)$ can not be obtained from $C_0(\hat{s}, m_H^2, m_t^2, m_t^2)$ by a simple substitution.

We also define the abbreviations

$$\begin{aligned} D_F(\hat{t}) &= m_H^2 D_0(\hat{t}) - (1-\beta z) C_0(\hat{t}, m_H^2, m_t^2, m_t^2), \\ D_F(\hat{u}) &= m_H^2 D_0(\hat{u}) - (1+\beta z) C_0(\hat{u}, m_H^2, m_t^2, m_t^2), \end{aligned} \tag{A.8}$$

where $\beta = (1-4m_t^2/\hat{s})^{1/2}$ and $z = (\hat{\mathbf{P}}_g \cdot \hat{\mathbf{P}}_t)$, together with the UV-finite combination

$$\begin{aligned} \mathcal{B} = {} & 9\beta z[B_0(\hat{t}, m_H^2, m_t^2) - B_0(\hat{u}, m_H^2, m_t^2)] + 18z^2[B_0(\hat{s}, m_t^2, m_t^2) - B_0(m_t^2, m_H^2, m_t^2)] \\ & + 7[B_0(\hat{t}, m_H^2, m_t^2) + B_0(\hat{u}, m_H^2, m_t^2) - 2B_0(m_t^2, m_H^2, m_t^2)], \end{aligned} \tag{A.9}$$

and (see [3])

$$C_s(\hat{t}) = C_0(\hat{t}, m_H^2, m_t^2, m_t^2) + \frac{B_0(m_t^2, m_H^2, m_t^2) - B_0(\hat{t}, m_H^2, m_t^2)}{m_t^2 - \hat{t}}, \tag{A.10}$$

$$G(\hat{s}) = \frac{-[m_H^2 C_0(\hat{s}, m_H^2, m_t^2, m_t^2) + B_0(\hat{s}, m_t^2, m_t^2) - B_0(m_t^2, m_H^2, m_t^2)]}{\hat{s}\beta^2}. \tag{A.11}$$

Furthermore, $C_s(\hat{u})$ is obtained from eq. (A.10) by the replacement $\hat{t} \to \hat{u}$. The factor

$$\kappa = \frac{m_t^2\sqrt{2}\, G_F\, g_s^4}{8\pi^2}, \tag{A.12}$$

where g_s is the QCD coupling constant, determines the over-all scale.

The functions b_{g1}^{CP} and c_{g1} are odd under ($z \to -z$, implying $\hat{t} \to \hat{u}$) whereas b_{g2}^{CP} and c_{g2} are even. In the following, the four- and three-point functions are finite in four dimensions, as well as all combinations of two-point functions.

For the box diagram (diagram (c) in fig. 3), we find:

$$
\begin{aligned}
b_{g_1}^{(c)} &= \kappa\,\gamma_{CP}\,\frac{-m_t\,E_1}{192(1-\beta^2z^2)(1-z^2)\hat{s}\beta} \\
&\times\Big[(7+9\beta z)\Big(2z[\,\hat{s}\,(1-\beta z)^2+4m_H^2]\,\mathrm{Im}\,D_F(\hat{t}) \\
&\qquad +\{\hat{s}\beta z[\hat{s}\beta(1-\beta z)(1-2\beta z+z^2)+4m_H^2(\beta-z)] \\
&\qquad -\hat{s}^2\beta(1-\beta z)(1-\beta^2)\}\,\mathrm{Im}\,D_0(\hat{t})\Big)-(z\to -z;\ \hat{t}\to\hat{u}) \\
&+4\beta^2 z\big[\hat{s}(7-18\beta^2z^2+7z^2)-18m_H^2z^2(3-z^2)-9\hat{s}(1-\beta^2)\big]\mathrm{Im}\,C_0(\hat{s},m_H^2,m_t^2,m_t^2) \\
&+4z\big[\hat{s}(7-11\beta^2z^2)+28m_H^2\big]\mathrm{Im}\,C_0(\hat{s},m_t^2,m_t^2,m_t^2)-4\beta^2z(1-z^2)\mathrm{Im}\,\mathcal{B}\Big], \qquad \text{(A.13)}\\
b_{g_2}^{(c)} &= \kappa\,\gamma_{CP}\,\frac{m_t}{192(1-\beta^2z^2)(1-z^2)\hat{s}\beta} \\
&\times\Big[(7+9\beta z)\big(2[\,\hat{s}\,(1-\beta z)^2+4m_H^2][(1-z^2)m_t+E_1z^2]\,\mathrm{Im}\,D_F(\hat{t}) \\
&\quad +\{\hat{s}\beta[\hat{s}\beta(1-\beta z)(1-2\beta z+z^2)+4m_H^2(\beta-z)][(1-z^2)m_t+E_1z^2] \\
&\quad -\hat{s}^2E_1\beta z(1-\beta z)(1-\beta^2)\}\,\mathrm{Im}\,D_0(\hat{t})\big)+(z\to -z;\ \hat{t}\to\hat{u}) \\
&+4\beta^2\big\{[\hat{s}(7-18\beta^2z^2+7z^2)-18m_H^2z^2(3-z^2)][(1-z^2)m_t+E_1z^2] \\
&\quad -18z^2m_t[m_H^2(1-z^2)+2m_tE_1]\big\}\mathrm{Im}\,C_0(\hat{s},m_H^2,m_t^2,m_t^2) \qquad \text{(A.14)}\\
&+4[\hat{s}(7-11\beta^2z^2)+28m_H^2][(1-z^2)m_t+E_1z^2]\mathrm{Im}\,C_0(\hat{s},m_t^2,m_t^2,m_t^2) \\
&-4\beta^2(1-z^2)[(2-z^2)m_t+E_1z^2]\mathrm{Im}\,\mathcal{B}\Big],
\end{aligned}
$$

$$
\begin{aligned}
c_{g_1}^{(c)} &= \kappa\,\gamma_{CP}\,\frac{m_t\,E_1}{192(1-\beta^2z^2)(1-z^2)\hat{s}\beta} \\
&\times\Big[(7+9\beta z)\big\{2z[\,\hat{s}\,(\beta^2z^2+2\beta^2-2\beta z-1)+4m_H^2]\,\mathrm{Re}\,D_F(\hat{t}) \\
&\qquad +\{\hat{s}\beta z[\hat{s}\beta(1-\beta z)(1-2\beta z+z^2)+4m_H^2(\beta-z)] \\
&\qquad +\hat{s}^2\beta(1-\beta z)(1-\beta^2)\}\,\mathrm{Re}\,D_0(\hat{t})\big\}-(z\to -z;\ \hat{t}\to\hat{u}) \qquad \text{(A.15)}\\
&+4\beta^2z\big[\hat{s}(7-18\beta^2z^2+7z^2)-18m_H^2z^2(3-z^2)+9\hat{s}(1-\beta^2)\big]\mathrm{Re}\,C_0(\hat{s},m_H^2,m_t^2,m_t^2) \\
&-4z\big[\hat{s}(7+11\beta^2z^2)-28m_H^2-14\hat{s}\beta^2\big]\mathrm{Re}\,C_0(\hat{s},m_t^2,m_t^2,m_t^2)-4\beta^2z(1-z^2)\mathrm{Re}\,\mathcal{B}\Big], \\
c_{g_2}^{(c)} &= \kappa\,\gamma_{CP}\,\frac{-m_t}{192(1-\beta^2z^2)(1-z^2)\hat{s}\beta} \\
&\times\Big[(7+9\beta z)\big(2\{[\hat{s}(\beta^2z^2-2\beta z-1)+4m_H^2][(1-z^2)m_t+E_1z^2]+2\hat{s}E_1\beta^2z^2\}\mathrm{Re}\,D_F(\hat{t}) \\
&\quad +\{\hat{s}\beta[\hat{s}\beta(1-\beta z)(1-2\beta z+z^2)+4m_H^2(\beta-z)][(1-z^2)m_t+E_1z^2]
\end{aligned}
$$

$$
\begin{aligned}
&+\hat{s}^2E_1\beta z(1-\beta z)(1-\beta^2)\}\,\mathrm{Re}\,D_0(\hat{t})\Big)+(z\to -z;\ \hat{t}\to\hat{u})\\
&+4\beta^2\big\{[\hat{s}(7-18\beta^2z^2+7z^2)-18m_H^2z^2(3-z^2)][(1-z^2)m_t+E_1z^2]\\
&\quad-18z^2m_t[m_H^2(1-z^2)-2m_tE_1]\big\}\mathrm{Re}\,C_0(\hat{s},m_H^2,m_t^2,m_t^2)\\
&-4\{[\hat{s}(7+11\beta^2z^2)-28m_H^2][(1-z^2)m_t+E_1z^2]-14\hat{s}E_1\beta^2z^2\}\mathrm{Re}\,C_0(\hat{s},m_t^2,m_t^2,m_t^2)\\
&-4\beta^2(1-z^2)[(2-z^2)m_t+E_1z^2]\mathrm{Re}\,\mathcal{B}.\Big]
\end{aligned}
\tag{A.16}
$$

From the vertex diagrams (d and e in fig. 3):

$$
\begin{aligned}
c_{g_1}^{(d+e)}&=\kappa\,\gamma_{CP}\,\frac{-m_t\,E_1}{96(1-\beta^2z^2)}\Big[(7+9\beta z)\Big(2(1-\beta^2)\;C_0(\hat{t},m_H^2,m_t^2,m_t^2)\\
&\qquad+\frac{\beta z}{1-\beta z}\;(1+\beta^2z^2-2\beta^2)\;C_s(\hat{t})\Big)-(z\to -z;\ \hat{t}\to\hat{u})\Big],
\end{aligned}
\tag{A.17}
$$

$$
\begin{aligned}
c_{g_2}^{(d+e)}&=\kappa\,\gamma_{CP}\,\frac{\beta\,m_t}{96(1-\beta^2z^2)}\Big[(7+9\beta z)\Big(\frac{2m_t}{E_1+m_t}(E_1+m_t-\beta zE_1)C_0(\hat{t},m_H^2,m_t^2,m_t^2)\\
&\qquad-\frac{m_t+E_1z^2-m_tz^2}{E_1^2(1-\beta z)}(E_1^2-2m_t^2-\beta^2E_1^2z^2)C_s(\hat{t})\Big)+(z\to -z;\ \hat{t}\to\hat{u})\Big].
\end{aligned}
$$

From the self-energy diagram (after fixing the signs):

$$
\begin{aligned}
c_{g_1}^{(f)}&=\kappa\,\gamma_{CP}\,\frac{-m_t}{192E_1(1-\beta^2z^2)}\\
&\quad\times\Big[(7+9\beta z)\frac{1-\beta^2}{1-\beta z}\Big(B_0(m_t^2,m_H^2,m_t^2)-B_0(\hat{t},m_H^2,m_t^2)\Big)-(z\to -z;\ \hat{t}\to\hat{u})\Big],\\
c_{g_2}^{(f)}&=\kappa\,\gamma_{CP}\,\frac{\beta\,m_t}{192(1-\beta^2z^2)}\Big[(7+9\beta z)\frac{m_t}{E_1+m_t}\frac{E_1+m_t-\beta zE_1}{E_1^2(1-\beta z)}\\
&\quad\times\Big(B_0(m_t^2,m_H^2,m_t^2)-B_0(\hat{t},m_H^2,m_t^2)\Big)+(z\to -z;\ \hat{t}\to\hat{u})\Big].
\end{aligned}
\tag{A.18}
$$

From diagram (g):

$$
\begin{aligned}
b_{g_2}^{(g)}&=\kappa\,\gamma_{CP}\,\frac{-3m_t^2\beta^3z^2\mathrm{Im}\,G(\hat{s})}{8(1-\beta^2z^2)}\\
c_{g_2}^{(g)}&=\kappa\,\gamma_{CP}\,\frac{3m_t^2\beta^3z^2\mathrm{Re}\,G(\hat{s})}{8(1-\beta^2z^2)}.
\end{aligned}
\tag{A.19}
$$

Finally, from diagram (h):

$$
\begin{aligned}
b_{g_2}^{(h)}&=\kappa\,\gamma_{CP}\,\frac{m_t^2}{(\hat{s}-m_H^2)^2+\Gamma_H^2m_H^2}\;\frac{-\beta}{4(1-\beta^2z^2)}\\
&\quad\times\Big[2m_t^2[\Gamma_Hm_H\mathrm{Re}\,C_0(\hat{s},m_t^2,m_t^2,m_t^2)-(\hat{s}-m_H^2)\mathrm{Im}\,C_0(\hat{s},m_t^2,m_t^2,m_t^2)]+\Gamma_Hm_H\Big],
\end{aligned}
\tag{A.20}
$$

$$c_{g_2}^{(h)} = \kappa\,\gamma_{CP}\,\frac{m_t^2}{(\hat{s}-m_H^2)^2+\Gamma_H^2 m_H^2}\Big[\frac{\beta}{16(1-\beta^2 z^2)}\Big(2\hat{s}(1+\beta^2) \tag{A.21}$$
$$\times[(\hat{s}-m_H^2)\mathrm{Re}\,C_0(\hat{s},m_t^2,m_t^2,m_t^2)+\Gamma_H m_H \mathrm{Im}\,C_0(\hat{s},m_t^2,m_t^2,m_t^2)]-4(\hat{s}-m_H^2)\Big)$$
$$+\frac{3}{32}\frac{m_t^2\sqrt{2}\,G_F}{8\pi^2}[2\hat{s}^3\beta\tilde{a}^2|C_0(\hat{s},m_t^2,m_t^2,m_t^2)|^2+2\hat{s}\beta a^2|2-\hat{s}\beta^2 C_0(\hat{s},m_t^2,m_t^2,m_t^2)|^2]\Big],$$

where Γ_H is the width of the Higgs boson calculated by summing the partial widths for $H\to W^+W^-, ZZ, t\bar{t}$ in the version of 2HDM we considered.

References

[1] C. R. Schmidt and M. E. Peskin, Phys. Rev. Lett. **69** (1992) 410.

[2] D. Atwood, A. Aeppli and A. Soni, Phys. Rev. Lett. **69** (1992) 2754.

[3] W. Bernreuther and A. Brandenburg, Phys. Rev. D **49** (1994) 4481 [arXiv:hep-ph/9312210].

[4] W. Bernreuther, A. Brandenburg and M. Flesch, CERN-TH/98-390, PITHA 98/41, arXiv:hep-ph/9812387.

[5] T. D. Lee, Phys. Rev. D **8** (1973) 1226;
G. C. Branco and M. N. Rebelo, Phys. Lett. B **160** (1985) 117;
J. Liu and L. Wolfenstein, Nucl. Phys. B **289** (1987) 1;
S. Weinberg, Phys. Rev. D **42** (1990) 860;
Y. L. Wu and L. Wolfenstein, Phys. Rev. Lett. **73** (1994) 1762 [arXiv:hep-ph/9409421].

[6] I. F. Ginzburg, M. Krawczyk and P. Osland, arXiv:hep-ph/0101208;
Nucl. Instrum. Meth. A **472** (2001) 149 [arXiv:hep-ph/0101229];
arXiv:hep-ph/0211371; and preprint CERN-TH/2003-020, to be published.

[7] R.K. Ellis, W.J. Stirling and B.R. Webber, *QCD and Collider Physics*, Cambridge University Press (Cambridge, 1996).

[8] K. S. Babu, C. F. Kolda, J. March-Russell and F. Wilczek, Phys. Lett. B **402** (1997) 367 [arXiv:hep-ph/9703299];
A. Pilaftsis, Phys. Lett. B **435** (1998) 88 [arXiv:hep-ph/9805373];
A. Pilaftsis and C. E. Wagner, Nucl. Phys. B **553** (1999) 3 [arXiv:hep-ph/9902371];
M. Carena, J. Ellis, S. Mrenna, A. Pilaftsis and C. E. Wagner, arXiv:hep-ph/0211467.

[9] C. R. Schmidt, Phys. Lett. B **293** (1992) 111.

[10] H. Y. Zhou, Phys. Rev. D **58** (1998) 114002 [arXiv:hep-ph/9805358].

[11] J. A. Vermaseren, Comput. Phys. Commun. **83** (1994) 45.

[12] J. Pumplin, D. R. Stump, J. Huston, H. L. Lai, P. Nadolsky and W. K. Tung, JHEP **0207** (2002) 012 [arXiv:hep-ph/0201195].

[13] T. Hahn and M. Perez-Victoria, Comput. Phys. Commun. **118** (1999) 153 [arXiv:hep-ph/9807565]. See also http://www.feynarts.de/looptools/

[14] G. J. van Oldenborgh and J. A. Vermaseren, Z. Phys. C **46** (1990) 425.

[15] B. Grzadkowski and W. Y. Keung, Phys. Lett. B **319** (1993) 526 [arXiv:hep-ph/9310286].

[16] B. Grzadkowski and J. Pliszka, Phys. Rev. D **63** (2001) 115010 [arXiv:hep-ph/0012110];
Acta Phys. Polon. B **32** (2001) 1919 [arXiv:hep-ph/0104011].

[17] For more details, see Wafaa Khater, Ph. D. thesis (University of Bergen, 2003).

[18] S. L. Glashow and S. Weinberg, Phys. Rev. D **15** (1977) 1958.

[19] G. C. Branco, L. Lavoura, J. P. Silva, "CP Violation" (Oxford Univ. Press, 1999).

[20] D. E. Groom *et al.* [Particle Data Group Collaboration], Eur. Phys. J. C **15** (2000) 1.

[21] J.F. Gunion, H.E. Haber, G. Kane, S. Dawson, *The Higgs Hunter's Guide* (Addison-Wesley, Reading, 1990).

[22] A. Mendez and A. Pomarol, Phys. Lett. B **272** (1991) 313.

[23] T. Hayashi, Y. Koide, M. Matsuda, M. Tanimoto and S. Wakaizumi, Phys. Lett. B **348** (1995) 489 [arXiv:hep-ph/9410413].

[24] A. Heister *et al.* [ALEPH Collaboration], Phys. Lett. B **526** (2002) 191 [arXiv:hep-ex/0201014]; J. Abdallah *et al.* [DELPHI Collaboration], Eur. Phys. J. C **23** (2002) 409 [arXiv:hep-ex/0201022]; P. Achard *et al.* [L3 Collaboration], Phys. Lett. B **517** (2001) 319 [arXiv:hep-ex/0107054]; G. Abbiendi *et al.* [OPAL Collaboration], arXiv:hep-ex/0209078; see also LEP Higgs Working Group, LHWG Note/2002-01 http://lephiggs.web.cern.ch/LEPHIGGS/www/Welcome.html

[25] P. Achard *et al.* [L3 Collaboration], Phys. Lett. B **545** (2002) 30 [arXiv:hep-ex/0208042].

[26] G. Abbiendi *et al.* [OPAL Collaboration], arXiv:hep-ex/0206022.

[27] J. L. Hewett and J. D. Wells, Phys. Rev. D **55** (1997) 5549 [arXiv:hep-ph/9610323]; D. Atwood, S. Bar-Shalom, G. Eilam and A. Soni, Phys. Rept. **347** (2001) 1 [arXiv:hep-ph/0006032].

[28] W. Bernreuther, A. Brandenburg, Z. G. Si and P. Uwer, Phys. Lett. B **509** (2001) 53 [arXiv:hep-ph/0104096];
W. Bernreuther, A. Brandenburg, Z. G. Si and P. Uwer, Phys. Rev. Lett. **87** (2001) 242002 [arXiv:hep-ph/0107086].

[29] A. Brandenburg, M. Flesch and P. Uwer, Phys. Rev. D **59** (1999) 014001 [arXiv:hep-ph/9806306].